Plant Soil (2016) 402:47–62
DOI 10.1007/s11104-015-2768-y

REGULAR ARTICLE

Surface-based GPR underestimates below-stump root biomass

John R. Butnor · Lisa J. Samuelson · Thomas A. Stokes · Kurt H. Johnsen · Peter H. Anderson · Carlos A. González-Benecke

Received: 10 August 2015 / Accepted: 2 December 2015 / Published online: 10 December 2015

Abstract
Aims While lateral root mass is readily detectable with ground penetrating radar (GPR), the roots beneath a tree (below-stump) and overlapping lateral roots near large trees are problematic for surface-based antennas operated in reflection mode. We sought to determine if tree size (DBH) effects GPR root detection proximal to longleaf pine (*Pinus palustris* Mill) and if corrections for could be applied to stand-level estimates of root mass.
Methods GPR (1500 MHz) was used to estimate coarse root mass proximal to 33 longleaf pine trees and compared to the amount of biomass excavated from pits proportional in area to tree basal diameter. Lateral roots were excavated to a depth of 1 m and taproots were excavated in their entirety.
Results GPR underestimated longleaf pine below-stump mass and the magnitude of the underestimation increased with tree DBH. Non-linear regressions between GPR estimated root mass/excavated root mass and tree diameter at breast height (DBH) were highly significant for both below-stump (lateral + taproot) root mass ($p < 0.0001$, R^2 0.77) and lateral coarse root mass ($p < 0.0001$, R^2 0.65).
Conclusions GPR underestimates root mass proximal to trees, and this needs to be accounted for to accurately estimate stand-level belowground biomass.

Keywords GPR · Root mass, taproot · Lateral root · Below-stump · *Pinus palustris* · Longleaf pine

Abbreviations

DBH	Diameter at breast height (cm) measured 1.4 m above ground level
GPR	Ground penetrating radar
MHz	Megahertz

Introduction

The most common way to estimate allocation to roots on a whole tree or stand level is through the development and application of allometric relationships, where easily

Responsible Editor: Peter J. Gregory.

J. R. Butnor (✉)
USDA Forest Service, Southern Research Station, 81 Carrigan Drive, Aiken Center, Room 208, University of Vermont, Burlington, VT 05405, USA
e-mail: jbutnor@fs.fed.us

K. H. Johnsen
USDA Forest Service, Southern Research Station, 1577 Brevard Road, Asheville, NC 28806, USA

L. J. Samuelson · T. A. Stokes
School of Forestry and Wildlife Sciences, Auburn University, 3301 SFWS Building, Auburn, AL 36849, USA

P. H. Anderson
USDA Forest Service, Southern Research Station, 3041 East Cornwallis Road, Durham, NC 27709, USA

C. A. González-Benecke
Department of Forest Engineering, Resources and Management College of Forestry, Oregon State University, 280 Peavy Hall, Corvallis, OR 97331, USA

measured parameters such as tree diameter and height are related to difficult to measure parameters such as: stem, branch, foliar, below-stump, taproot, or lateral root biomass (Ter-Mikaelian and Korzukhin 1997; Drexhage and Colin 2001; Jenkins et al. 2003). Allometric equations are indispensable for modeling forest production and carbon allocation, though they may be site specific and, contingent on climate, soil drainage, or available nutrients and stand structure; however, such equations may also be modified by factors such as latitude, stand basal area and density, and site index (Gonzalez-Benecke et al. 2014). Because it is difficult to conduct complete belowground harvests of a single tree with multiple nearby neighbors and overlapping lateral root systems, predefined pits or pits proportion to tree size are excavated at the base of the tree to capture the bulk of roots (Retzlaff et al. 2001; Samuelson et al. 2004; Albaugh et al. 2006; Samuelson et al. 2014). These allometric relationships do not account for roots beyond the excavation pit, which can be a significant omission in forests with widely dispersed individuals exploiting resources unevenly in large open gaps or competing with different size trees. Despite lower density, extensive roots are critical for accessing water and nutrient resources further from the tree (Stone and Kalisz 1991). For example, in mature longleaf pine (*Pinus palustris* Mill.) forests, roots have been reported to extend up to 9.3 m from the stem with total root lengths up to 12.2 m (Hodgkins and Nichols 1977), thus other approaches to augment models based on pit excavation are required.

For the past 15 years, ground penetrating radar (GPR) operated in frequencies between 400 and 2600 MHz has been evaluated and used as a tool to augment or replace destructive belowground sampling of lateral roots (Hruska et al. 1999; Butnor et al. 2001; Butnor et al. 2003; Barton and Montagu 2004; Stover et al. 2007; Butnor et al. 2012; Guo et al. 2013a). To collect such data, a GPR antenna comprised of an electromagnetic transmitter and receiver is pulled along a transect propagating electromagnetic waves into the soil at specific intervals (usually 100–200 per m) and the receiver precisely records the time of arrival and amplitude of energy that reflects off of buried objects and returns to the surface (A-scan). With knowledge of soil dielectric properties, the A-scans may be combined to form a two-dimensional profile (distance X depth) to create a radagram (B-scan), showing hyperbolic reflections from roots at given depths and relative amplitude along a transect (Fig. 1). Approaches that use signal

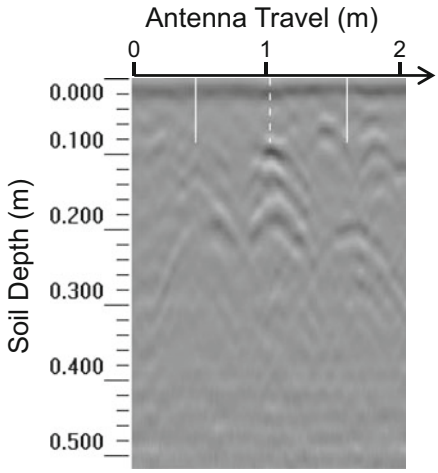

Fig. 1 Sample radargram (B-scan) from a 25 year-old stand longleaf pine stand in North Carolina. Numerous longleaf pine roots were detected and appear as hyperbolic reflections. At a distance of 1 m (*dashed line*), a 15 cm diameter soil corer was used to verify coarse root mass to a depth of 0.5 m. Total dry coarse root mass of the core was 61.2 g with two larger roots (1.1 and 4.3 cm diameter) recovered between soil depths of 10 and 20 cm

amplitude and image analysis processing can be used to rapidly quantify GPR data and relate high amplitude area (number of pixels above an amplitude threshold) to total coarse root mass and be used to create root biomass maps. High amplitude area is calibrated using soil cores or small excavations, so that excavated coarse root mass and area on an image file above some threshold may be correlated (Butnor et al. 2001; Butnor et al. 2003; Cox et al. 2005; Stover et al. 2007; Dannoura et al. 2008; Butnor et al. 2012; Day et al. 2013; Guo et al. 2013b; Borden et al. 2014). Other approaches that use waveform (A-scan) geometry are able to extract data from individual or stacked waveforms to calculate root depth, diameter or make estimates of biomass from root diameter (Barton and Montagu 2004; Dannoura et al. 2008; Hirano et al. 2009; Cui et al. 2011; Guo et al. 2013b). Root mapping may be achieved by algorithms that predict which roots are continuous or separate between adjacent scans. There have been many recent advances in geometric data interpretation, though the post-collection processing is still operator intensive and is often difficult to automate without some user guidance (Butnor et al. 2012; Guo et al. 2013a).

For GPR root surveys to be successful they need to be conducted on suitable soils that are not prone to signal attenuation (Doolittle et al. 2007). Sandy soils with low dielectric values are ideal, while high clay,

haline or wet soils are unsuited (Butnor et al. 2001; Daniels 2004; Doolittle et al. 2007). Variation in root water content (Hirano et al. 2009; Guo et al. 2013b) and root orientation relative to antenna travel may also limit accurate detection of root parameters (Tanikawa et al. 2013; Guo et al. 2015). Recently, Guo et al. (2015) proposed a novel method to correct for the effect of cross angle on amplitude area of a root reflection. As methods of GPR root surveys advance, it is important to recognize and mitigate other limitations of surface-based antennas. The soil volume directly beneath and adjacent to a tree is a problematic environment for root detection with surface-based GPR antennas operated in reflection mode, as vertical root detection is limited. Roots need to be located belowground, not protruding the soil surface and covered with only some minimum amount of soil to detect single or multiple reflections of electromagnetic waves from the soil/root interfaces. The most readily interpretable, hyperbolic root reflections come from lateral roots crossed at 90 degrees by a GPR antenna, with adequate soil volume above and below the root (Butnor et al. 2001; Barton and Montagu 2004; Tanikawa et al. 2013; Guo et al. 2015). Even if a taproot were cut below the soil surface and covered with soil, its location and basal area would be detected, but its vertical extension into the soil profile would not. Large overlapping lateral roots originating from vertically orientated taproot would also be difficult to detect due to interference from reflections from the first root, closest to the surface. Based on past field observations, it was expected that GPR would underestimate below-stump (taproot + lateral) root mass of trees that develop tap roots, though the magnitude of the underestimation is unknown. The issue of partial detection of below-stump root mass was raised by Samuelson et al. (2014) working with mature longleaf pine. While integrating below-stump biomass data from longleaf pine pit excavations with lateral root data from GPR, the lack of insight into where the two methods overlap lead to the consideration and averaging of two options. It was assumed that taproots were undetectable and either: 1) estimated total root mass = GPR root + excavated tap root or 2) estimated total root mass = GPR root + excavated tap root + excavated lateral root (Samuelson et al. 2014). The logic being that GPR detected all lateral roots adjacent to trees (1) or GPR detected none of the lateral roots adjacent to trees (2). If GPR detected all of the lateral roots adjacent to trees there would be overlap with pit excavations. This led to considerable uncertainty, as the bounds of these two scenarios were rather wide (Samuelson et al. 2014). For the purpose of belowground biomass accounting the average of the two detection scenarios was used, since there were no direct comparisons between GPR and pit excavations to guide the calculation. This need not detract from the usefulness of GPR for detecting coarse lateral roots, but is an important complexity to consider when scaling these values to the level of a forest stand, since using GPR data alone could greatly underestimate belowground biomass of trees. Preliminary reports of cross-hole tomography with borehole radar are promising, but have not materialized as a practical approach or had the necessary research and development for application of the technology (Butnor et al. 2006; Butnor et al. 2012).

We compared root mass estimated with GPR (1500 MHz) in a defined area at base of 33 longleaf pine trees ranging in DBH from 4.0 to 54.3 cm with excavated root mass to determine if tree size effects accuracy of root detection under field conditions. While it has been assumed that taproots are not detectable with surface-based GPR, the detectability of lateral roots proximal to trees had not been quantified. Information on root detectability near trees is needed to better integrate whole tree biomass harvests with extensive GPR surveys further away from trees. This is particularly important for species that develop large taproots (e.g. *Pinus* sp.) or have large overlapping lateral roots originating from the vertically orientated taproot. Once the relationship between tree size (DBH) and root detection was established for longleaf pine, it was applied to correct stand-level root mass estimates from 20 longleaf plots (Samuelson et al. 2014).

Materials and methods

Study sites

The locations selected for study represent the east-west range of longleaf pine from Marine Corps Base Camp Lejeune, near Jacksonville, North Carolina on the Atlantic coast to the Kisatchie National Forest, near Leesville, in west-central Louisiana. A total of eight even-aged stands ranging in age from 8 to 83 years old were selected on soils suitable for GPR surveys (Table 1). The Louisiana soils were sandy loams and sandy clay loams that were suited to shallow surveys in

the upper 50 cm above heavy clay horizons, while the coarse sands in the North Carolina were ideal for GPR (Doolittle et al. 2007). Within the eight stands, a wide variety of tree sizes were selected; DBH ranged from 4.0 to 54.3 cm and tree heights ranged from 2.3 to 30.4 m (Table 1).

Calibration of GPR with soil cores

At each stand, a set of 1 cm diameter aluminum rods were driven horizontally into undisturbed soil at depths of 10, 20, 30, 40 cm via an access trench (subsequently re-filled) in order to estimate soil dielectric value using a SIR-3000 radar unit (Geophysical Survey Systems Inc., Nashua, NH, USA) connected to a 1500 MHz antenna. The dielectric value varies with soil mineralogy and moisture content and was used to scale two-way travel time of reflected energy to predicted depth. Stand specific dielectric and range values are listed in Table 2. All GPR data were collected at 140 scans per m, 512 samples per scan, and 16 bits per sample with FIR (boxcar) collection filter and gain settings of −20, 15, 30. To directly compare image-based GPR indices with root biomass, a total of 25 locations in each stand were carefully marked, scanned with the 1500 MHz antenna and a 15 cm diameter core was used to collect roots to a depth of 50 cm. Within each stand, a subsample point was located at the center and three additional subsample points were located 35 m distant at 0, 120, 240 degrees from north following the protocol of Law et al. (2008). Soil cores were located 2 m away from each subsample point at 0, 90, 180, 270 degrees from north. The 16 cores (4 cores X 4 subplots) were chosen without regard to tree proximity, giving them similar distribution attributes to random soil core samples i.e. many soil cores with low to moderate root contents, very few with large root content. To develop regressions that relate GPR observations to biomass it was necessary to populate the calibration data with a full range of root biomass from low to high rather than to obtain a normal distribution which would not be achieved without a very large sample. An additional 9 cores were located by surveying for areas of low and high root mass a priori with GPR. In this manner, an additional 3 low root mass and 6 high root mass "radar-guided" core locations were selected. Roots were washed free of soil, classified as live or dead and separated into size classes (<2 mm, 2–10 mm, >10 mm. Roots were dried to constant mass at 65 °C and weighed.

Radar data were processed and scaled to biomass using methods described by Butnor et al. (2012) and summarized with the following steps:

1. Post-collection processing of GSSI GPR radargrams (*.dzt) was performed with RADAN 7.0 software (Geophysical Survey Systems Inc., Nashua, NH, USA). All files received position correction and background removal to remove planar (horizontal)

Table 1 Descriptive site and study tree parameters for the eight *Pinus palustris* stands where GPR coarse root mass surveys were compared to excavation

Year Sampled	Location & Stand Age (years)	Origin	Latitude, Longitude	Ele. (m)	Soil texture	*n*	Mean DBH (cm)	DBH range (cm)	Mean Height (m)	Height range (m)	Mean pit area (m^2)
Louisiana											
2013	8	Planted	30.94529, −93.16255	70	Sandy loam	5	7.0	4.0–11.2	5.1	2.3–11.2	1.04
2013	18	Planted	30.94140, −93.19137	67	Sandy loam	4	12.8	4.6–23.4	9.8	4.4–13.2	1.20
2013	34	Planted	30.99211, −93.13294	87	Sandy clay loam	5	21.8	11.0–33.3	17.8	14.6–22.1	1.53
2013	60	Planted	30.99756, −93.01920	78	Sandy clay loam	3	36.8	31.7–42.8	23.1	21.9–24.8	2.30
2013	83	Planted	31.02399, −92.94459	84	Sandy clay loam	3	49.4	45.9–54.3	28.2	26.6–30.4	3.42
North Carolina											
2014	15	Planted	34.58873–77.27051	5	Sand	5	16.2	9.5–22.7	10.5	8.7–12.5	1.19
2014	25	Planted	34.64346, −77.45200	21	Sand	5	15.4	8.0–22.5	12.0	7.6–14.8	1.22
2014	79	Natural Regen.	34.69979, −77.30035	10	Sand	3	41.9	28.8–54.3	21.6	19.4–25.8	2.67

reflections from soil horizons and surfaces. Extra gain was applied radargrams on stands with particularly low amplitude if necessary.

2. Root location was spatially corrected using Kirchoff migration to reduce multiple reflections and help identify the geometry of a hyperbolic reflectors (Oppenheim and Schafer 1975; Berkhout 1981; Daniels 2004) The results were compared with the Hilbert transformation (Butnor et al. 2003; Stover et al. 2007), where the magnitude of the phase of the signal is transformed and reflectors may be revealed by reducing multiple reflections. In most cases the Hilbert transform alone was used, and at one stand the Hilbert transform was applied after migration and extra gain to resolve faint reflectors (Table 2).
3. Processed *.dzt files converted to 8-bit grayscale bitmap image files.
4. Images were analyzed with an intensity threshold to determine the relative proportion of the image populated with root reflections using SigmaScan Pro Image Analysis Software (Systat Software, Point Richmond, CA). The threshold range is highly dependent on root and soil properties and is manually determined intensity threshold range will by focusing on small roots (~1 cm diameter) and comparing resolution of different threshold values (0 is black, 255 is white), usually within the range of 60–200.
5. The entire radargram image is parsed into sections representative of a 15 cm soil core and the number of "high-amplitude" pixels above the threshold are tallied for each individual "virtual core", i.e. 15 m transect would be sectioned in 100 images, that would be tallied separately with SigmaScan.
6. The dry mass of live roots (g) in series of soil cores is compared with the number of high amplitude pixels or area using regression analysis. The resulting equation is applied to pixel tallies from virtual cores to estimate root mass at specific locations

Below-stump root biomass estimation with GPR

A 4 m by 4 m square (16 m^2) centered on each sample tree was designated for GPR surveying prior to excavation. The surface was raked clear of litter and woody debris, then a series of 9 parallel lines, 4 m long, spaced 0.5 m apart were established with ground marking paint. The transects were scanned with a 1500 MHz antenna connected to a SIR-3000 GPR unit using system settings

Table 2 System settings for the SIR-3000 radar unit equipped with a 1500 MHz antenna and post-collection data processing parameters

Location & stand age	Soil Water Con. (%)	Soil Dielectric (unitless)	Scan/m	Range (ns)	Collection Filters	Post-Collection Filters				Image Analysis	
						Pos. Corr.	Back. Rem.	Mig.	Hilbert Trans.	Extra Gain	Amplitude Threshold	Correlation Coeff. (r) with soil cores
Louisiana												
8	18.0	8	140	14	FIR (boxcar), gain −20, 15, 30	✓	✓		✓		140	0.69
18	14.8	8	140	14	FIR (boxcar), gain −20, 15, 30	✓	✓		✓		136	0.89
34	11.5	7	140	14	FIR (boxcar), gain −20, 15, 30	✓	✓		✓		136	0.84
60	11.3	8	140	14	FIR (boxcar), gain −20, 15, 30	✓	✓		✓		140	0.85
83	26.6	10	140	18	FIR (boxcar), gain −20, 15, 30	✓	✓		✓		136	0.89
North Carolina												
15	5.8	7	140	14	FIR (boxcar), gain −20, 15, 30	✓	✓		✓		140	0.79
25	4.5	6	140	14	FIR (boxcar), gain −20, 15, 30	✓	✓	✓	✓	✓	136	0.77
79	4.3	5	140	14	FIR (boxcar), gain −20, 15, 30	✓	✓		✓		135	0.74

presented in Table 2. As the center line (line 5) cannot go through the tree, the antenna was advanced to the base of the tree, then followed the circumference (to the right) and resuming a straight path on the other side of the tree.

The GPR data were processed as previously described, though prior to image analysis (steps 4–6), reflections from debris related to military exercises (shell casings, wire, metal foil) were parsed from the images. Unwanted reflections from metallic objects were readily identified, having either very high amplitude or "ringing" parallel reflections throughout the profile. Less than 10 % of each radargram was omitted. After image analysis was complete, the lowest denominator for spatial distribution was the amount of root mass predicted in a 15 cm^2 core to a depth of 50 cm expressed as g/m^2, kg/m^2 or Mg/ha depending on the relevant scale at hand. Along each transect, a root mass value was calculated every 15 cm, resulting in 9 lines, 50 cm apart containing 28 observations each, for a total of 252 observations per tree (16 m^2). These data were used to create a root biomass distribution map for the entire 16 m^2 area around each tree where the x, y coordinates are linked to root mass values. The data were summarized as the total amount of root mass predicted in the excavation area (1 to 4 m^2) that varied with tree size (described in the next section). The root mass data were also analyzed as a function of distance from the center of the tree, where the tree centered at (2 m, 2 m) was adjusted to the origin (0 m, 0 m) by subtracting 2 from both the x and y coordinates of all 252 observations. The distance between the center of the tree and the root mass estimate was calculated with the Pythagorean equation where:

$$x^2 + y^2 = \text{distance } to \text{ center of tree}^2 \quad (1)$$

In order to better understand the relationship between accuracy of GPR detection of lateral roots and tree proximity, 11 trees across the range of DBH were scanned with GPR at a distance of 0.5, 1 and 1.5 m from the outer edge of the tree and cored for verification. These 33 soil cores are separate from the cores used to calibrate GPR to provide some core-based validation of the GPR results within the excavation pit.

Harvest of below-stump coarse root biomass

After GPR surveying was complete, trees were felled and a square excavation area (pit) centered on the stump was designated. It had been common practice to sample below-stump root mass (lateral + taproot) in loblolly pine (*Pinus taeda* Mill) by designating a fixed area e. g. 1 m^2 centered on the tree, and excavate the full extent of the taproot (Retzlaff et al. 2001; Samuelson et al. 2004; Albaugh et al. 2006). The standard 1 m^2 pit had previously been applied to trees as old as 18 years (Albaugh et al. 2006), but was considered too small for large trees in the present study (up to 83 years old). It was not feasible to excavate and follow the full extent of all roots in the field; hence a variable pit area proportional to tree size was used. The minimum pit area for the smallest trees was 1 m^2 (trees < ~10 cm DBH) and the maximum was 4 m^2. The specific area of each pit was calculated from the linear relationship between tree basal diameter (ground-level) to objectively link variable pit area with tree size (Samuelson et al. 2014). Pit area may also be approximated using DBH (cm) where: pit area (m^2) = 0.8322 $e^{0.0301 * DBH}$; $R^2 = 0.95$, $p < 0.001$. Mean pit areas by stand are presented in Table 1.

We define below-stump coarse root mass as taproot mass (cut at ground-level) and all mass from lateral roots >5 mm diameter within the excavation pit. Lateral coarse roots (> 5 mm) were excised from the taproot and cut cleanly at pit walls to a depth of 1 m. The excavated soil was sieved through hardware cloth (0.63 cm mesh) and all longleaf pine roots >5 mm in diameter were collected. The entire taproot was removed either manually or with a mini-excavator. All roots were washed free of soil and dried to constant mass at 65 °C.

Statistical analysis

Root mass estimated by GPR within the excavation pit (1–4 m^2) was compared to below-stump mass (taproot + lateral) and lateral root mass excavated from each of the 33 trees. Data were analyzed using SAS for Windows 9.4 (SAS Institute, Cary, NC). Regression analysis was used to predict the ratio of GPR root detection (coarse root mass estimated with GPR: excavated coarse root mass) in the excavation pit using tree DBH. As data were collected at two geographically distinct regions (western Louisiana and eastern North Carolina), the F-test for extra sum of squares was applied to determine if the regions had similar regression parameters and could be pooled. The resulting p value was >0.1 for both below-stump and lateral root mass models so the

Louisiana and North Carolina data were pooled. Specific regression models were selected based on analysis of residuals and R^2 values. Mixed model analysis was used to examine the relationship between tree DBH and allocation of root mass to taproots within the excavated pit.

Results

The linear relationships between lateral coarse root mass collected via soil cores and GPR index (high amplitude area) had correlation coefficients (r) between 0.69 and 0.89 for each the eight stands (Table 2). These regressions were site specific, dependent on soil and root properties and soil moisture at the time of sampling. A total 14 cores were uninterpretable from high soil water content and 32 contained metallic debris from military training and were omitted from the analysis. Regression equations were developed using the remaining 156 core scans to predict the amount of root mass in each core (Fig. 2). The 95 % confidence interval largely included the 1:1 line, demonstrating the relative accuracy of GPR lateral root biomass estimates ($R^2 = 0.72$, $p < 0.0001$). The y-intercept (6.94 g root mass) of regression line did not pass through zero as a minimum amount of root mass was needed for detection (Fig. 2).

To help visualize rooting density in the excavation pit as well as entire 16 m^2 area around a tree, root biomass maps from four trees ranging in DBH from 8 to 54.3 cm are presented as contour plots (Fig. 3). The maps are not intended to reveal details of root architecture; rather detectability of roots near trees in stand-level surveys. These maps show that detection of roots with GPR near the base of the tree and within the area designated for excavation was suppressed. GPR underestimated below-stump root mass and the magnitude increased with tree size. For the examples in Fig. 3: 64 % of below-stump root mass was detected near the smallest tree (8.0 cm DBH; Fig. 3a), while only 5 % was detected proximal to the largest tree (54.3 cm DBH, Fig. 3d) (Table 3). Due to the vertical orientation of the taproot, it was unlikely that GPR is detecting much of the taproot mass. If it is assumed that the taproot is undetectable and GPR results are compared with lateral roots excavated from the pits, the proportion detected increased markedly (Table 3).

The relationship between GPR root detection (GPR estimated/excavated root mass) in the excavation pits and tree DBH was analyzed using non-linear regression. Using data from all 33 trees, the portion of root mass in the pit detected by GPR and tree DBH were highly significant for both lateral root mass ($p < 0.0001$, $R^2 = 0.65$) and below-stump root mass ($p < 0.0001$, $R^2 = 0.77$) (Fig. 4). GPR overestimated lateral coarse root mass on small longleaf pine trees (DBH <10 cm) and underestimated on trees >10 cm DBH (Fig. 4a). Less than 13 % of the lateral coarse root mass of the two largest trees (both 54.3 cm DBH) was detected with GPR. Below-stump root mass was largely underestimated by GPR and the ratio of GPR estimated to excavated root mass decreased sharply

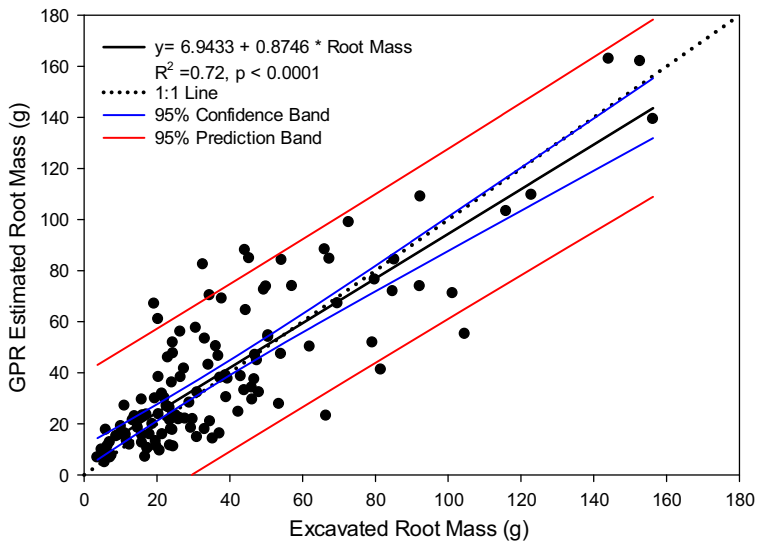

Fig. 2 Comparison of excavated and GPR estimated root mass from 15 cm diameter soil cores to a depth of 50 cm. Dry root mass is presented as g per core

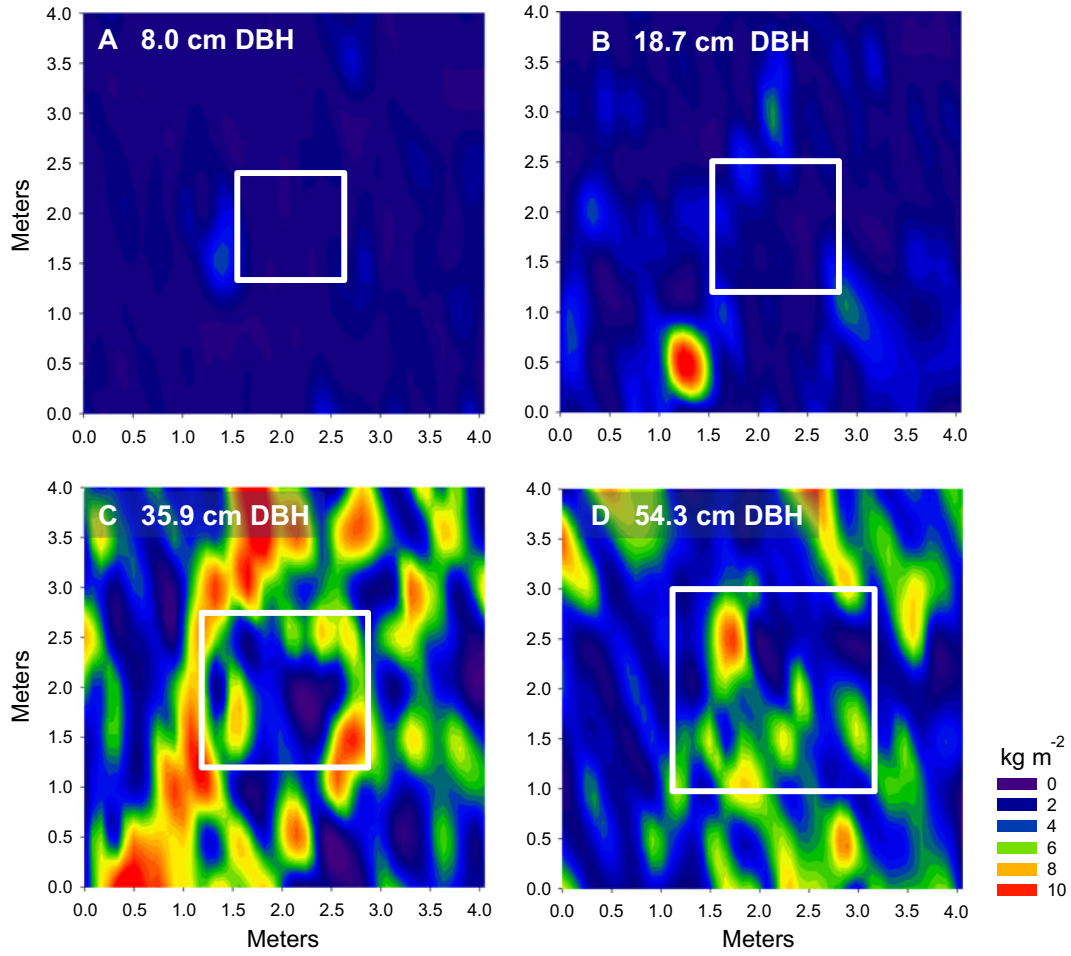

Fig. 3 Root biomass maps (16 m^2) generated using GPR data from four trees representing the range of tree DBH analyzed **a** 8.0 cm, **b** 18.7 cm, **c** 35.9 cm and **d** 54.3 cm. The *white outlines* indicate the excavation area. Tree parameters are summarized in Table 3

with tree diameter (Fig. 4b). At diameters of >15 cm, less than 20 % of below-stump mass was detectable with GPR.

Pooling all data from North Carolina and Louisiana (n = 33); 67 % of the root biomass in the pit was attributed to the taproot. Allocation of root mass to taproot in trees with DBH < 10 cm was significantly lower than the 10–20, 20–30, 30–40 cm DBH classes ($F = 6.58$, $p = 0.0004$). There were no significant differences between the other DBH classes. Allocation to taproot by DBH intervals is presented in Table 4. Even if it is assumed that GPR is not detecting taproots that comprise the majority of below-stump root mass, laterals roots are still being underestimated proximal

Table 3 Predicted and excavated root mass associated with root biomass maps in Fig. 3

DBH (cm)	Height (m)	Age (years)	Root detected with GPR in pit (kg)	Lateral root excavated (kg)	Taproot excavated (kg)	Below-stump excavated (kg)	Lateral roots detected (%)	Below-stump detected (%)
8.0	7.6	25	1.2	0.9	1.0	1.9	132	64
18.7	14.4	25	3.5	5.6	25.0	30.6	62	11
35.9	24.8	60	19.9	25.3	140.3	165.6	78	12
54.3	25.8	79	26.5	211.0	305.9	516.9	13	5

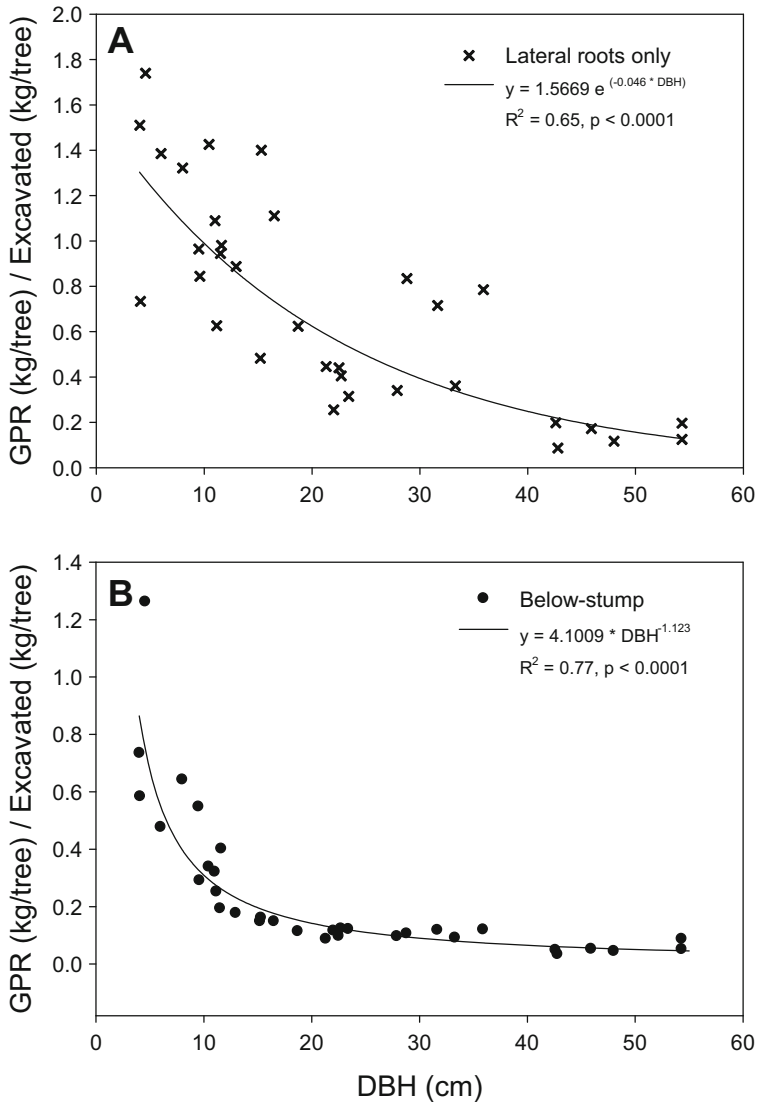

Fig. 4 Regression analysis of GPR root detection in the excavation pit (mass estimated (kg/tree)/mass excavated (kg/tree)) with tree DBH for 33 longleaf pine trees in Louisiana and North Carolina. Separate regressions were made for lateral roots (**a**) and below-stump (tap + lateral roots) (**b**). Overestimation of lateral roots with GPR occurred adjacent to small longleaf pine (<10 cm dbh) followed by underestimation of lateral roots adjacent to larger trees (**a**). Below-stump (tap + lateral roots) mass was overestimated with GPR for one tree (4.6 cm dbh), followed by underestimation of lateral roots adjacent to remaining trees (**b**)

to trees (Fig. 4) and this is at odds with the relative agreement between GPR estimates and excavated root mass from soil cores (Fig. 2). Eleven of the 33 trees were surveyed with GPR at a distance of 0.5, 1 and 1.5 m from the outer edge of the stem and GPR estimates were compared to excavated root mass from soil cores (Fig. 5). At a distance of 0.5 m from the tree, the proportion of roots detected declined with DBH, though the effect was not significant at 1.0 or 1.5 m (Fig. 5). Despite being a small sample, this supports the supposition that GPR calibration equations developed away from trees will underestimate root mass near trees and this effect will lessen as the distance from the tree widens.

Root mass detected with GPR in the entire16 m^2 sample area was plotted as distance from tree to illustrate root distribution within and beyond the excavation pit (Fig. 6a). The data are not normally distributed as they were collected in parallel lines and expressed as the radius from the center of the tree (Fig. 6b). Data were averaged by DBH class (<10, 10–20, 20–30, 30–40, 40–50, >50 cm) resulting in 252 mass/distance observations per class (Fig. 6a). For comparison, mean lateral root mass recovered via pit excavation for each DBH interval was 1.10, 2.31, 6.64, 11.40, 41.30 and 41.02 kg m^{-2}, respectively. The smallest DBH class (<10 cm) shows a gradual increase in root mass closer to the tree and good agreement between GPR and excavated lateral root

Table 4 Proportion of *Pinus palustris* coarse root biomass attributed to the taproot compared with published values of several *Pinus* species. Age and DBH are denoted either as a mean or an age interval depending on the study

Species	Location	n	Age (yrs)	DBH (cm)	Taproot:total root biomass (%)	Reference
Pinus palustris	Louisiana and North Carolina	7	13	< 10	46	Based on excavation data from present study, all data pooled by DBH
		10	19	10–20	75	
		7	31	20–30	72	
		3	66	30–40	81	
		4	78	40–50	67	
		2	81	50–60	57	
Pinus pinaster	S.W. France (maritime)	30		10–20	45	Augusto et al. (2015), taproot includes stump.
		25		20–30	40	
		17		30–60	30	
Pinus pinea	Italy (coastal)	14	50–62	24–39	57	Cutini et al. (2013)
Pinus resinosa	Michigan (Western Upper P.)	*	5	5	85	Calculated from: King et al. (2007), taproot includes stump 30 cm above ground line. **260 total trees harvested across all ages*
			8	6	90	
			12	10	80	
			17	14	68	
			32	17	82	
			22	18	89	
			55	25	64	
Pinus sylvestris	Finland (southern)	7	34	9–20	30	Calculated from: Vanninen et al. (1996), taproot includes stump.
		5	65	20–30	27	
		3	121	30–40	35	
		3	169	40–50	33	
Pinus taeda	South Carolina (upper piedmont)	15	48	30	55	Vanlear and Kapeluck (1995) *combination of harvest and modeling*

mass near the tree. The next two intervals (10–20 and 20–30 cm) show similar patterns, though root mass detected near the tree is 1.4 to 3.7 times lower than excavated root mass. Trees >30 cm DBH show a marked increase in root detection between 2.5 and 1.5 m from the tree were they appear to be in close agreement, near the tree lateral root mass is underestimated between 3.1 and 11 times.

Discussion

Direct comparison between GPR estimates and excavated root mass at the base of trees demonstrated that GPR underestimates below-stump root mass and the degree of underestimation is related to tree size (DBH). This in opposition to comparisons between GPR estimates of lateral root mass and verification with soil cores (that were not proximal trees) which were in close agreement. The footprint of the antenna is an inverted cone, with some limited ability for side-scanning (Conyers and Goodman 1997), this may be a factor with small trees (<10 cm DBH) where there is adequate soil volume to coarse root mass near the base of the tree. The overestimation of lateral root mass observed on small trees may result from the taproot being detected as additional lateral roots, as radargrams did not show any deep reflections consistent with vertical taproots.

Our findings contrast with those reported by Borden et al. (2014) who scanned a 20.25 m^2 area around 25 year old trees of five tree species in southern Ontario, Canada (12 trees total) with a 1000 MHz GPR antenna and compared the results to excavations to a depth of 1 m. When pooled across species, GPR estimates and excavation were within 1 % of each other.

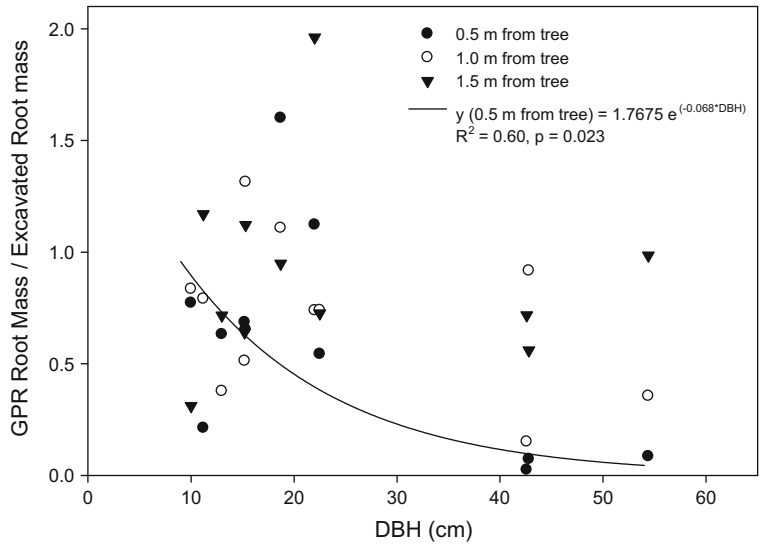

Fig. 5 Regression of the proportion of roots detected with GPR (verified with soil cores) at distances of 0.5, 1.0 and 1.5 m from and tree DBH for 11 of the 33 sample trees

When considered by species, GPR estimates by Borden et al. (2014) for *Juglans nigra* L. (n = 2) and *Quercus rubra* L. (n = 3) were in close agreement with excavation data, underestimates were reported for *Populus* sp. (32 %, n = 2) and *Thuja occidentalis* L. (16 %, n = 3) and overestimates for *Picea abies* L. Karst (24 %, n = 2). While underestimation of root mass is anticipated with deep or vertical roots, it was observed to a lesser degree by Borden et al. (2014). The authors explained that some of the detected biomass may be from false positives and that with the exception of *Populus* sp., these trees tended to have more readily detectable horizontal roots. Roots were not classified as horizontal and vertical (taproot), so further quantitative assessment is not possible. Key differences with the present study are: 1) the excavation area was 20.25 m^2 versus our variable 1–4 m^2 pits and the larger area may dilute any underestimates proximal to the tree, 2) pine species have a tendency for tap or sinker roots and thus root morphology of pine is very different than the species examined by Borden et al. (2014), and 3) use of a 1000 MHz center frequency antenna would afford deeper penetration, but have less ability to detect smaller roots (<1.5 cm) than the 1500 MHz antenna used in the present study.

Longleaf pine has some similarities in root morphology and below-stump allocation of biomass with the other major southern yellow pines (*Pinus taeda* L.; *Pinus elliottii* Engelm.; *Pinus echinata* Mill.) and other *Pinus* sp. that develop a taproot or a cluster of vertical roots beneath the tree. Tree root biomass harvests are conducted to develop allometric equations, though few published reports describe the percent allocation to lateral and tap roots. Data from the present study are compared to reported values for other *Pinus* sp. in Table 4. Over half of the root biomass in *P. palustris*, *Pinus pinea* L., *Pinus resinosa* Ait. and *P. taeda* are allocated to taproots while approximately one third is allocated to taproots in *Pinus pinaster* Ait. and *Pinus sylvestris* L. (Table 4). This is a considerable amount of coarse root mass that GPR is unlikely to detect, especially in mature trees, and thus needs to be explicitly accounted for when scaling GPR-based data to the stand level. With some parameterization, the equations in Fig. 4 could be adapted for other *Pinus* sp. so that spatial analysis of root distribution GPR could be used in conjunction with below-stump allometry. It seems likely that GPR would underestimate coarse root mass proximal to mature trees of other genera; more so with deep, vertical rooting patterns and less with shallow rooting patterns. Globally, temperate coniferous forests have an average root: shoot ratio of 0.18 with over 50 % of the root mass located in the upper 30 cm of soil (Jackson et al. 1996), making it important to mitigate this potential for underestimation proximal to trees with GPR. An analysis by Robinson (2007) cites evidence that root biomass is widely underreported and could be as much as 68 % greater on a global basis. It is possible that current estimates of belowground biomass in many forests are underrepresenting extensive roots further away from trees and wider adoption of GPR protocols could help mitigate this. Thus, GPR remains an important tool to estimate stand-level root biomass.

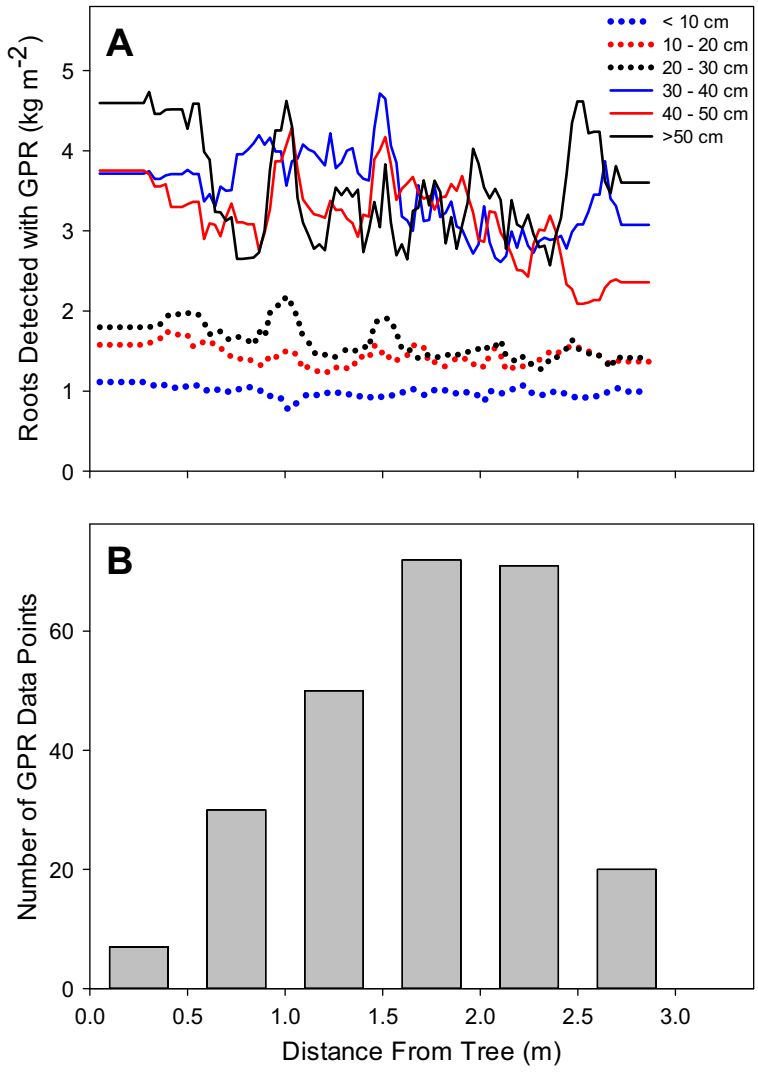

Fig. 6 Root mass detected with GPR in the entire16 m^2 sample area plotted as distance from tree (**a**). Data were averaged by DBH class (<10, 10–20, 20–30, 30–40, 40–50, >50 cm) resulting in 252 mass/distance observations per class. The data were smoothed using a running average filter with a sampling proportion of 0.05. The distribution of GPR data points as related to distance from tree are presented in inset B

The need for the present study became apparent while conducting stand level surveys of ecosystem C pools in longleaf stands in Georgia (Samuelson et al. 2014), Louisiana and North Carolina. Surveying root mass with GPR on the scale of hundreds or thousands of square meters per day necessitates wider transect spacing for expediency and may preclude gridding in multiple angles that would be applied in root architecture studies. While less detailed than close spaced gridded data collection (e.g. 25 cm grid, (Zenone et al. 2008), 10 cm grid (Borden et al. 2014)), a 10 by 10 m plot scanned at 0.5 m line spacing and mass estimates every 15 cm still affords over 1400 root mass observations in 100 m^2, which is rather comprehensive and would be prohibitive to sample otherwise via destructive methods. The single tree plots were sampled at the same density as stand level surveys so they could be used to correct for near tree bias. While detectability of below-stump root mass by GPR within defined pit areas is highly predictable and the accuracy of GPR lateral root detections away from trees is very good, our study design is limited in determining were the two metrics intersect. With limited core validation in the present study, it can only be speculated that by 1.5 m away from large longleaf pine the underestimation by GPR is abated. This leaves some ambiguity, which would have been better addressed by making many more comparisons of GPR and soil cores at a finer scale (e.g. 0–4 m from tree at 0.25 m intervals).

In a study of 20 longleaf pine stands aged 5 to 87 years in Georgia, USA, Samuelson et al. (2014) estimated belowground live root C using a combination of allometry and GPR. They developed allometric equations with tree height and DBH to predict below-stump mass from the harvest of 21 trees using the same variable pit area method as the present study (1–4 m^2). Stand inventory data (tree height, DBH) from the 20 plots was used to estimate stand-level below-stump biomass that was expressed as Mg C ha^{-1} (root mass * carbon concentration). At the center of each plot a 100 m^2 subsample was surveyed with GPR to estimate stand-level lateral root C (Mg C ha^{-1}). As the potential for overlap or "double counting" of root mass between allometric modeling of below-stump mass and GPR lateral root surveys was unknown, stand level live root C was calculated two ways: 1) estimated total root C = GPR lateral root C + taproot C (allometric modeling), and 2) estimated total root C = GPR root + taproot C (allometric modeling) + lateral root C (allometric modeling). This led to uncertainty when analyzing ratios of above- and belowground C allocation, at maximum aboveground C of 100 Mg C·ha^{-1}, belowground C varied by 20 % (Samuelson et al. 2014). We recalculated the GPR estimates of lateral roots reported

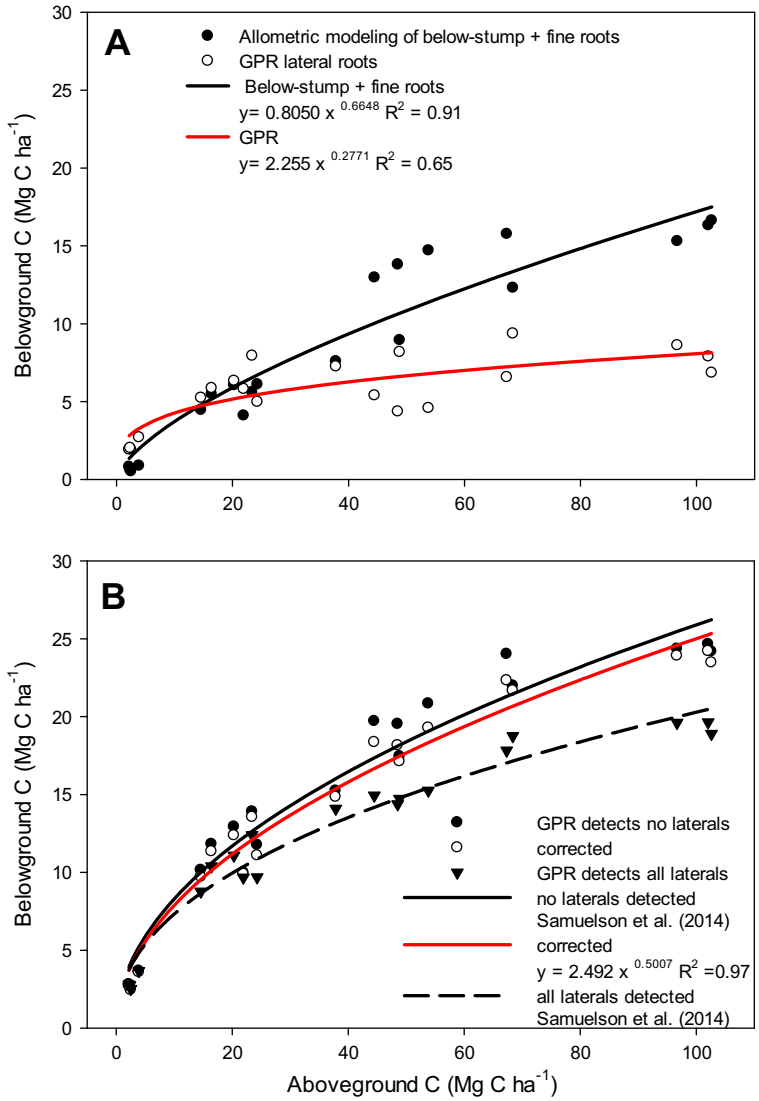

Fig. 7 Comparison of above- and belowground C from 20 plots of longleaf pine aged 5 to 87 years in Georgia (Samuelson et al. 2014) where lateral root C (GPR) is presented separate from below-stump C plus fine roots (allometric modelling) (**a**). Stand-level lateral root C (GPR) and below-stump mass plus fine roots (allometric modelling) were combined to calculate total root C (**b**). These data were originally reported by Samuelson et al. (2014) with assumptions of *no lateral roots are detected by GPR in the below-stump sample area* and *all lateral roots are detected by GPR in the below-stump sample area.* The lateral root (GPR) C data were corrected for below-stump underestimation using the approach and equation (Fig. 4b) described in the present study

by Samuelson et al. (2014) using inventory data with the following steps:

1) Calculated the below-stump mass of each tree via allometric equations (Samuelson et al. 2014)
2) Determined the ratio of below-stump mass detected by GPR for that tree (Fig. 4b):

$$\left(\text{GPR mass}/\text{excavated mass} = 4.1009 \bullet \text{DBH}^{-1.123}\right)$$

3) Calculated the amount of below-stump mass per tree that was estimated by both allometry and GPR per tree (overlap between methods)
4) Converted biomass to C content by multiplying by below-stump C concentration
5) Deducted this amount from the GPR stand-level estimate of lateral root C.

Using this approach we obtained stand-level estimates of lateral root C (detected with GPR) for each plot separate from estimates of stand-level below-stump C (allometric modeling) + fine root C. Lateral root C (detected with GPR) increased with aboveground C for the 20 longleaf pine plots and represented 34 % of the belowground C pool at maximum aboveground C (100 Mg C ha-1) compared with 66 % attributed to below-stump C + fine root C (allometric modeling) (Fig. 7a). Stand-level lateral root C (GPR) was then added to below-stump C + fine root C (allometric modeling) to obtain a corrected value for total belowground C (Fig.7b). Since the taproot and large overlapping roots near the trunk of the tree make up the bulk of below-stump root C and are widely underestimated by GPR, it is logical that corrected belowground C estimate is closer to the assumption that GPR detected no lateral roots in the excavated pits (Fig. 7b). While GPR underestimates below-stump root mass, it does account for roots between and away from trees that would otherwise go unaccounted for using only allometric modeling based on excavation pits. Across the range of stand ages (5 to 87 years) analyzed by Samuelson et al. (2014), GPR accounted for 67 % of the belowground C in the youngest and 34 % in the oldest stand (Fig. 7a).

Conclusions

When using GPR-based data to scale coarse root mass to the stand level, it is critical to account for the portion of mass directly under and adjacent to trees that is not measureable by surface-based antennas. Although GPR can accurately measure lateral coarse root mass under suitable soil conditions, the proportion of below-stump mass detected with GPR declined sharply with tree diameter. We would expect similar below-stump mass underestimation with other species that develop large taproots and associated proximal lateral roots, particularly in older stands with large trees. For example, many pine species allocate more than half of root mass to vertical taproots or sinker roots. Thus, accurate scaling of GPR-based coarse root mass data to the stand level requires integration with allometric modeling of below-stump mass.

Acknowledgments This research was supported by the U. S. Department of Defense through the Strategic Environmental Research and Development Program (SERDP). We appreciate the technical support provided by Jake Blackstock, Joel Burley, Thomas Christensen, Robert Eaton, Shelly Hooke, Jason Jackson, Lance Kress, John Lewis, Michael Rameriz, Justin Rathel and Karen Sarsony. We thank Dr. Frank Day, Old Dominion University, for reviewing this manuscript prior to submission.

References

Albaugh TJ, Allen HL, Kress LW (2006) Root and stem partitioning of Pinus taeda. Trees 20:176–185. doi:10.1007/s00468-005-0024-4

Augusto L, Achat DL, Bakker MR, Bernier F, Bert D, Danjon F, Khlifa R, Meredieu C, Trichet P (2015) Biomass and nutrients in tree root systems-sustainable harvesting of an intensively managed Pinus pinaster (Ait.) planted forest. Global Change Biology Bioenergy 7:231–243. doi:10.1111/gcbb.12127

Barton CVM, Montagu KD (2004) Detection of tree roots and determination of root diameters by ground penetrating radar under optimal conditions. Tree Physiol 24:1323–1331

Berkhout AJ (1981) Wave field extrapolation techniques in seismic migration, a tutorial. Geophysics 46:1638–1656. doi:10.1190/1.1441172

Borden KA, Isaac ME, Thevathasan NV, Gordon AM, Thomas SC (2014) Estimating coarse root biomass with ground penetrating radar in a tree-based intercropping system. Agrofor Syst 88:657–669. doi:10.1007/s10457-014-9722-5

Butnor JR, Doolittle JA, Kress L, Cohen S, Johnsen KH (2001) Use of ground-penetrating radar to study tree roots in the southeastern United States. Tree Physiol 21:1269–1278

Butnor JR, Doolittle JA, Johnsen KH, Samuelson L, Stokes T, Kress L (2003) Utility of ground-penetrating radar as a root biomass survey tool in forest systems. Soil Sci Soc Am J 67:1607–1615

Butnor JR, Johnsen KH, Wikstrom P, Lundmark T, Linder S (2006) Imaging tree roots with borehole radar. 11th International Conference on Ground Penetrating Radar, Columbus Ohio

Butnor JR, Barton CVM, Day FP, Johnsen KH, Mucciardi AN, Schroeder RE, Stover DB (2012) Using ground-penetrating radar to detect tree roots and estimate biomass. In: Mancuso S (ed) Measuring roots: an updated approach. Springer, Heidelberg, New York

Conyers LB, Goodman D (1997) Ground-penetrating radar: an introduction for archaeologists. AltaMira Press, Walnut Creek

Cox KD, Scherm H, Serman N (2005) Ground-penetrating radar to detect and quantify residual root fragments following peach orchard clearing. HortTechnology 15:600–607

Cui XH, Chen J, Shen JS, Cao X, Chen XH, Zhu XL (2011) Modeling tree root diameter and biomass by ground-penetrating radar. Sci China-Earth Sci 54:711–719. doi:10.1007/s11430-010-4103-z

Cutini A, Chianucci F, Manetti MC (2013) Allometric relationships for volume and biomass for stone pine (Pinus pinea L.) in Italian coastal stands. iForest 6:7. doi:10.3832/ifor0941-006

Daniels DJ (2004) Ground penetrating radar. Institution of Electrical Engineers, London

Dannoura M, Hirano Y, Igarashi T, Ishii M, Aono K, Yamase K, Kanazawa Y (2008) Detection of cryptomeria japonica roots with ground penetrating radar. Plant Biosyst 142:375–380. doi:10.1080/11263500802150951

Day FP, Schroeder RE, Stover DB, Brown ALP, Butnor JR, Dilustro J, Hungate BA, Dijkstra P, Duval BD, Seiler TJ, Drake BG, Hinkle CR (2013) The effects of 11 yr of CO2 enrichment on roots in a Florida scrub-oak ecosystem. New Phytol 200:778–787. doi:10.1111/nph.12246

Doolittle JA, Minzenmayer FE, Waltman SW, Benham EC, Tuttle JW, Peaslee SD (2007) Ground-penetrating radar soil suitability map of the conterminous United States. Geoderma 141:416–421. doi:10.1016/j.geoderma.2007.05.015

Drexhage M, Colin F (2001) Estimating root system biomass from breast-height diameters. Forestry 74:491–497. doi:10.1093/forestry/74.5.491

Gonzalez-Benecke CA, Gezan SA, Albaugh TJ, Allen HL, Burkhart HE, Fox TR, Jokela EJ, Maier CA, Martin TA, Rubilar RA, Samuelson LJ (2014) Local and general above-stump biomass functions for loblolly pine and slash pine trees. For Ecol Manag 334:254–276. doi:10.1016/j.foreco.2014.09.002

Guo L, Chen J, Cui XH, Fan BH, Lin H (2013a) Application of ground penetrating radar for coarse root detection and quantification: a review. Plant Soil 362:1–23. doi:10.1007/s11104-012-1455-5

Guo L, Lin H, Fan BH, Cui XH, Chen J (2013b) Impact of root water content on root biomass estimation using ground penetrating radar: evidence from forward simulations and field controlled experiments. Plant Soil 371:503–520. doi:10.1007/s11104-013-1710-4

Guo L, Wu Y, Chen J, Hirano Y, Tanikawa T, Li WT, Cui XH (2015) Calibrating the impact of root orientation on root quantification using ground-penetrating radar. Plant Soil 395:289–305. doi:10.1007/s11104-015-2563-9

Hirano Y, Dannoura M, Aono K, Igarashi T, Ishii M, Yamase K, Makita N, Kanazawa Y (2009) Limiting factors in the detection of tree roots using ground-penetrating radar. Plant Soil 319:15–24. doi:10.1007/s11104-008-9845-4

Hodgkins EJ, Nichols NG (1977) Extent of main lateral roots in natural longleaf pine as related to position and age of trees. For Sci 23:161–166

Hruska J, Cermak J, Sustek S (1999) Mapping tree root systems with ground-penetrating radar. Tree Physiol 19:125–130

Jackson RB, Canadell J, Ehleringer JR, Mooney HA, Sala OE, Schulze ED (1996) A global analysis of root distributions for terrestrial biomes. Oecologia 108:389–411. doi:10.1007/bf00333714

Jenkins JC, Chojnacky DC, Heath LS, Birdsey RA (2003) National-scale biomass estimators for United States tree species. For Sci 49:12–35

King JS, Giardina CP, Pregitzer KS, Friend AL (2007) Biomass partitioning in red pine (pinus resinosa) along a chronosequence in the upper peninsula of Michigan. Can J For Res 37:93–102. doi:10.1139/x06-217

Law B, Arkebauer T, Campbell JL, Chen J, Sun O, Shwartz M, van Ingen C, Verma S (2008) Terrestrial carbon observations: protocols for vegetation sampling and data submission. Terrestrial Carbon Observations (TCO) Panel of the Global Terrestrial Observing System (GTOS). FAO, Rome

Oppenheim AV, Schafer RW (1975) Digital signal processing. Prentice Hall, Englewood Cliffs

Retzlaff WA, Handest JA, O'Malley DM, McKeand SE, Topa MA (2001) Whole-tree biomass and carbon allocation of juvenile trees of loblolly pine (Pinus taeda): influence of genetics and fertilization. Can J For Res 31:960–970

Robinson D (2007) Implications of a large global root biomass for carbon sink estimates and for soil carbon dynamics. Proc R Soc B Biol Sci 274:2753–2759. doi:10.1098/rspb.2007.1012

Samuelson LJ, Johnsen K, Stokes T (2004) Production, allocation, and stemwood growth efficiency of Pinus taeda L. stands in response to 6 years of intensive management. For Ecol Manag 192:59–70. doi:10.1016/j.foreco.2004.01.005

Samuelson LJ, Stokes TA, Butnor JR, Johnsen KH, Gonzalez-Benecke CA, Anderson P, Jackson J, Ferrari L, Martin TA, Cropper WP (2014) Ecosystem carbon stocks in pinus palustris forests. Can J For Res 44:476–486. doi:10.1139/cjfr-2013-0446

Stone EL, Kalisz PJ (1991) On the maximum extent of tree roots. For Ecol Manag 46:59–102. doi:10.1016/0378-1127(91)90245-q

Stover DB, Day FP, Butnor JR, Drake BG (2007) Effect of elevated Co-2 on coarse-root biomass in Florida scrub detected by ground-penetrating radar. Ecology 88:1328–1334. doi:10.1890/06-0989

Tanikawa T, Hirano Y, Dannoura M, Yamase K, Aono K, Ishii M, Igarashi T, Ikeno H, Kanazawa Y (2013) Root orientation can affect detection accuracy of ground-penetrating radar. Plant Soil 373:317–327. doi:10.1007/s11104-013-1798-6

Ter-Mikaelian MT, Korzukhin MD (1997) Biomass equations for sixty-five north American tree species. For Ecol Manag 97:1–24. doi:10.1016/S0378-1127(97)00019-4

Vanlear DH, Kapeluck PR (1995) Above and below-stump biomass and nutrient content of a mature loblolly-pine plantation. Can J For Res 25:361–367. doi:10.1139/x95-040

Vanninen P, Ylitalo H, Sievanen R, Makela A (1996) Effects of age and site quality on the distribution of biomass in scots

pine (Pinus sylvestris L). Trees 10:231–238. doi:10.1007/bf02185674

Zenone T, Morelli G, Teobaldelli M, Fischanger F, Matteucci M, Sordini M, Armani A, Ferre C, Chiti T, Seufert G (2008) Preliminary use of ground-penetrating radar and electrical resistivity tomography to study tree roots in pine forests and poplar plantations. Funct Plant Biol 35:1047–1058. doi:10.1071/fp08062